Supplementary Material for: Quantum Exceptional Chamber Induced by Large Nondipole Effect of a Quantum Dot Coupled to a Nano-Plasmonic Resonator

Yu-Wei Lu,* Renming Liu, Rongbin Su, and Xue-Hua Wang†
State Key Laboratory of Optoelectronic Materials and Technologies, School of Physics, Sun Yat-sen University, Guangzhou 510275, China

Jing-Feng Liu*
College of Electronic Engineering, South China Agricultural University, Guangzhou 510642, China.
(Dated: May 2019)

The Supplementary Material is organized as follows. Sec. I is the theoretical framework for the spontaneous emission of two-level quantum emitter based on macroscopic QED with multipole expansion. The evaluation of the multipole moments are summarized in Sec. II. Sec. III and IV are devoted to the details for the numerical simulation of LDOS and the convergence of the multipole expansion, respectively. Sec. V demonstrates that the exceptional point in the quantum system can be accessed by rotating the mesoscopic QD with nondipole effect. Sec. VI gives the conditions of forming a three-order EP by coupling two QDs to nanoshell. In Sec. VII, we briefly study the nondipole effect induced by the non-spherical QDs.

I. SPONTANEOUS EMISSION FROM QUANTUM DOT WITH MULTIPOLE EXPANSION

We start from the minimal coupling Hamiltonian [1]

$$H=\frac{1}{2m}(\boldsymbol{p}-e\boldsymbol{A})^2+e\varphi+U+\int d\boldsymbol{r}\int d\omega\hbar\omega\left(\hat{f}^{\dagger}(\boldsymbol{r},\omega)\hat{f}(\boldsymbol{r},\omega)+\frac{1}{2}\right) \tag{S1}$$

where m and e are the mass and charge of the electron, respectively. $\boldsymbol{p}$ is the canonical momentum operator, $\boldsymbol{A}$ and φ are the vector and scalar potentials of electromagnetic field, respectively. U is the binding potential and set to be zero. $\hat{f}(\boldsymbol{r},\omega))$ and $\hat{f}^{\dagger}(\boldsymbol{r},\omega))$ are the annihilation and creation operators of the quantized electromagnetic field, respectively. With Coulomb gauge $\nabla\cdot\boldsymbol{A}=0$ which implies $[\boldsymbol{p},\boldsymbol{A}]=0$ in quantum mechanics [2], the interaction Hamiltonian is

$$H_{int}=-\frac{e}{m}\boldsymbol{A}\cdot\boldsymbol{p}+e\varphi \tag{S2}$$

where we have omitted the term regarding $\boldsymbol{A}^2$ because it is a second-order process. Using the formalism of macroscopic QED [1], the vector and scalar potential are given by

$$\boldsymbol{A}(\mathbf{r},\omega)=\sqrt{\frac{\hbar}{\pi\varepsilon_0}}\frac{\omega}{c^2}\int d\mathbf{r}'\sqrt{\mathrm{Im}\left[\varepsilon\left(\mathbf{r}',\omega\right)\right]}\mathbf{G}^{\perp}\left(\mathbf{r},\mathbf{r}',\omega\right)\hat{f}\left(\mathbf{r}',\omega\right) \tag{S3}$$

$$\nabla\varphi(\mathbf{r},\omega)=-i\sqrt{\frac{\hbar}{\pi\varepsilon_0}}\frac{\omega^2}{c^2}\int d\mathbf{r}'\sqrt{\mathrm{Im}\left[\varepsilon\left(\mathbf{r}',\omega\right)\right]}\mathbf{G}^{\parallel}\left(\mathbf{r},\mathbf{r}',\omega\right)\hat{f}\left(\mathbf{r}',\omega\right) \tag{S4}$$

where $\mathbf{G}^{\perp}\left(\mathbf{r},\mathbf{r}',\omega\right)$ and $\mathbf{G}^{\parallel}\left(\mathbf{r},\mathbf{r}',\omega\right)$ are the transverse and longitudinal Green's function, respectively. According to $\mathbf{E}=-\nabla\varphi-\dot{\boldsymbol{A}}$, the electric field operator $\hat{\mathbf{E}}(\mathbf{r})$ can be expressed as

$$\widehat{\mathbf{E}}(\mathbf{r})=i\sqrt{\frac{\hbar}{\pi\varepsilon_0}}\int_0^{\infty}d\omega\int d^3\mathbf{r}'\frac{\omega^2}{c^2}\sqrt{\mathrm{Im}\left[\varepsilon\left(\mathbf{r}',\omega\right)\right]}\mathbf{G}\left(\mathbf{r},\mathbf{r}',\omega\right)\hat{f}\left(\mathbf{r}',\omega\right) \tag{S5}$$

where the dyadic Green's function $\mathbf{G}\left(\mathbf{r},\mathbf{r}',\omega\right)=\mathbf{G}^{\perp}\left(\mathbf{r},\mathbf{r}',\omega\right)+\mathbf{G}^{\parallel}\left(\mathbf{r},\mathbf{r}',\omega\right)$ denotes the electric field with frequency ω at $\mathbf{r}$ response to a point source located at $\mathbf{r}'$. The definition of the dyadic Green's tensor $\mathbf{G}\left(\mathbf{r},\mathbf{r}',\omega\right)$ is the solution of the wave equation with a point source at position $\mathbf{r}'$

$$\boldsymbol{\nabla}\times\boldsymbol{\nabla}\times\mathbf{G}\left(\mathbf{r},\mathbf{r}',\omega\right)-\left(\frac{\omega}{c}\right)^2\varepsilon(\mathbf{r},\omega)\mathbf{G}\left(\mathbf{r},\mathbf{r}',\omega\right)=\mathbf{I}\delta\left(\mathbf{r}-\mathbf{r}'\right) \tag{S6}$$

---

* These authors contributed equally
† Corresponding Author: wangxueh@mail.sysu.edu.cn

where $\mathbf{I}$ is the unit tensor. We use the QD notations that an electron can be either in the conduction band or in the valence band, denoting $|c\rangle$ and $|v\rangle$, respectively. Then the atomic raising and lowering operators can be recovered by $\sigma_- = |v\rangle\langle c|$ and $\sigma_+ = |c\rangle\langle v|$. Expanding the interaction Hamiltonian H_{int} on the complete set of electronic states $I = |c\rangle\langle c| + |v\rangle\langle v|$, the H_{int} in the interaction picture with rotating wave approximation is

$$H_{int} = -\frac{e}{m}\left(e^{i(\omega-\omega_0)t}\sigma_- \left\langle v\left|\widehat{\mathbf{E}}^{\dagger}(\mathbf{r})\cdot\boldsymbol{p}\right|c\right\rangle + H.c.\right) \tag{S7}$$

where ω_0 is the atomic transition frequency. Note that the commutators $[\mathbf{r}, H_0] = i\hbar\boldsymbol{p}/m$ is used to covert the position representation to momentum representation for scalar potential φ. Here the spatial variation of electromagnetic field over the wave function of QD is non-negligible, thus the electric field operator cannot be pulled out of the matrix element like that in dipole approximation, i.e., $\left\langle v\left|\widehat{E}_i^{\dagger}(\mathbf{r}_0)\,p_i\right|c\right\rangle \rightarrow \widehat{E}_i^{\dagger}(\mathbf{r}_0)\,\mu_i$, where $\mu_i = \langle v|p_i|c\rangle$ is the matrix element of dipole transition. We also consider the effect of a QD rotation along the direction of dipole transition, as illustrated in Fig. S1, by applying the unitary transformation $\widehat{U}_x(\phi) = e^{-(i/h)\hat{L}_x\phi}$ to H_{int}. Then one can calculate the transition matrix elements by Taylor expanding the electric field operator around the $\mathbf{r}_0$

$$\widehat{E}_i(\mathbf{r},\phi) = \widehat{E}_i(\mathbf{r}_0) + r_j(\phi)\times\partial_j\widehat{E}_i(\mathbf{r})|_{\mathbf{r}=r_0} + \frac{1}{2}r_k(\phi)r_j(\phi)\times\partial_k\partial_j\widehat{E}_i(\mathbf{r})|_{\mathbf{r}=\mathbf{r}_0} + \cdots \tag{S8}$$

where i,j,k represent the coordinate components, and $(\mathbf{r}-\mathbf{r}_0)_i$ has been replaced by r_i for simplicity. We keep the expansion to second order and rewrite the interaction Hamilton as

$$H_{int} = -\sum_{i,j,k} e^{i(\omega-\omega_0)t}\sigma_-\left(\mu_i(\phi)\hat{E}_i^{\dagger}(\mathbf{r}_0) + \Lambda_{ji}(\phi)\partial_j\hat{E}_i^{\dagger}(\mathbf{r}_0) + \Omega_{kji}(\phi)\partial_k\partial_j\widehat{E}_i^{\dagger}(\mathbf{r}_0)\right) + H.c. \tag{S9}$$

where $\mu_i(\phi) = (e/m)\langle v|p_i(\phi)|c\rangle|$, $\Lambda_{ji}(\phi) = (e/m)\langle v|r_j(\phi)p_i(\phi)|c\rangle$ and $\Omega_{kji}(\phi) = (e/2m)\langle v|r_k(\phi)r_j(\phi)p_i(\phi)|c\rangle$ are defined as the equivalent dipole, quadrupole and octupole transition moments in the momentum representation, respectively. From Eq. (S5) we can see that the electric field operator is related to the dyadic Green's function by the relationship $\int d^3s\frac{\omega^2}{c^2}\sqrt{\mathrm{Im}[\varepsilon(\mathbf{s},\omega)]}\mathbf{G}(\mathbf{r},s,\omega)\mathbf{G}^*(\mathbf{r}',\mathbf{s},\omega) = \mathrm{Im}[\mathbf{G}(\mathbf{r},\mathbf{r}',\omega)]$, and hence the Taylor expanding of electric field operator is equivalent to that of dyadic Green's function $\mathbf{G}(\mathbf{r},\mathbf{r}',\omega)$, which is

$$\mathbf{G}(\mathbf{r},\mathbf{r}') \cong \mathbf{G}(\mathbf{r}_0,\mathbf{r}_0) + \zeta\cdot J[\mathbf{G}(\mathbf{r},\mathbf{r}')]|_{(r_0,r_0)} + \frac{1}{2}\zeta^T\cdot H[\mathbf{G}(\mathbf{r},\mathbf{r}')]|_{(r_0,r_0)}\cdot\zeta \tag{S10}$$

where $\zeta = (\mathbf{r}-\mathbf{r}_0)$, J and H are the Jacobian matrix and Hessian matrix, respectively.

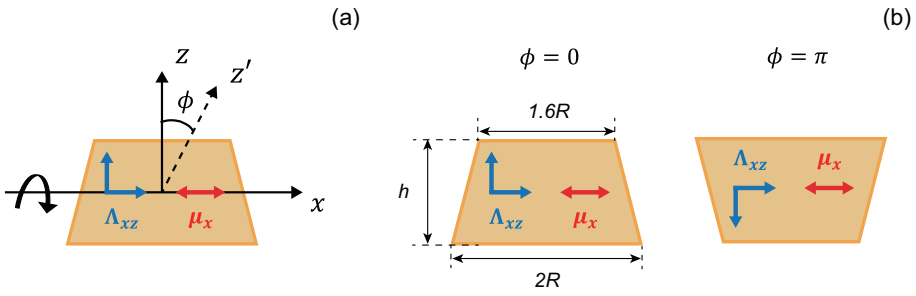

FIG. S1. (a) Rotation of a QD along the direction of its dipole transition (x axis). x and z are coordinate axis before rotation while z' are the new axis of z after a rotation, with the angle ϕ between them. (b) $\phi = 0$ corresponds to directed structure while $\phi = \pi$ is inverted structure.

The temporal evolution of the system at time t can be obtained by solving Schrödinger equation with the following wave function

$$|\Psi(t)\rangle = C_e(t)|c,0\rangle + \int d^3r\int_0^{\infty} d\omega C_g(\mathbf{r},\omega,t)|v,1(\mathbf{r},\omega)\rangle \tag{S11}$$

where $|c,0\rangle$ represents an electron is promoted to the conduction band and there is no photon in the surrounding, $|v,1(\mathbf{r},\omega)\rangle$ is the state that the transition of an electron from conduction band to valence band generates a photon in the surrounding. For spontaneous emission, the initial conditions are $C_e(0) = 1$ and $C_g(\mathbf{r},\omega,0) = 0$. Therefore, the evolution equations of probability amplitude $C_e(t)$ and $C_g(\mathbf{r},\omega,t)$ are

$$\dot{C}_e(t) = -\int_0^{\infty} d\omega\sqrt{\frac{1}{\hbar\pi\varepsilon_0}}\frac{\omega^2}{c^2}\int d^3\mathbf{r}'\sqrt{\mathrm{Im}[\varepsilon(\mathbf{r}',\omega)]}\sum_{i,j,k}\widehat{\Xi}^*_{i,j,k}[G_{ij}(\mathbf{r},\mathbf{r}',\omega)]\,C_g(\mathbf{r},\omega,t)e^{-i(\omega-\omega_0)t} \tag{S12}$$

$$\dot{C}_g(\mathbf{r},\omega,t)=\sqrt{\frac{1}{\hbar\pi\varepsilon_0}}\frac{\omega^2}{c^2}\sqrt{\mathrm{Im}\left[\varepsilon\left(\mathbf{r}',\omega\right)\right]}\sum_{i,j,k}\hat{\Xi}_{i,j,k}\left[G^*_{ij}\left(\mathbf{r},\mathbf{r}',\omega\right)\right]C_e(t)e^{i(\omega-\omega_0)t} \tag{S13}$$

where $\hat{\Xi}_{i,j,k}[\cdot]\equiv\mu_i+\Lambda_{ji}(\phi)\partial_j+\Omega_{kji}(\phi)\partial_j\partial_k$. Using one-sided Fourier transformation, the explicit solutions of $C_e(t)$ in frequency domain can be expressed as [3, 4]

$$C_e(\omega)=\frac{\frac{\Gamma(\mathbf{r}_0,\omega,\phi)}{2}}{\left[(\omega-\omega_0)-\Delta\left(\mathbf{r}_0,\omega,\phi\right)\right]^2+\left[\frac{\Gamma(\mathbf{r}_0,\omega,\phi)}{2}\right]^2} \tag{S14}$$

with

$$\Gamma\left(\mathbf{r}_0,\omega,\phi\right)=\frac{2\omega^2}{\hbar\varepsilon_0c^2}\sum_{i,j,k}\hat{\Xi}^2_{i,j,k}\left[\mathrm{Im}\left[G_{ij}\left(\mathbf{r}_0,\mathbf{r}_0,\omega\right)\right]\right] \tag{S15}$$

$$\Delta\left(\mathbf{r}_0,\omega,\phi\right)=\frac{1}{2\pi}\wp\int\frac{\Gamma\left(\mathbf{r}_0,\omega',\phi\right)}{\omega-\omega'}d\omega' \tag{S16}$$

where $\wp$ denotes the principal value. $C_e(\omega)$ is known as the spontaneous emission (SE) spectrum or polarization spectrum. $\Gamma\left(\mathbf{r}_0,\omega,\phi\right)$ and $\Delta\left(\mathbf{r}_0,\omega,\phi\right)$ are the local coupling strength (LCS) and level shift, respectively. The temporal dynamics $C_e(t)$ can be obtained by Fourier transforming $C_e(\omega)$. Since no Markovian approximation has been made, the results are valid in both weak and strong coupling regime.

One may also concern about the influence of multipolar transitions on coupling coefficient g, since Rabi splitting appears when the coupling strength of plasmon-exciton interaction is greater than the dissipation. For a point-like emitter $\hbar g=-\mathbf{E}\left(\mathbf{r}_0\right)\cdot\boldsymbol{d}$, where $\mathbf{E}\left(\mathbf{r}_0\right)$ is the classical electric field at the location of dipole $\mathbf{r}_0$, and $\mathbf{d}$ is the dipole moment. Then the coupling coefficient beyond the dipole approximation $\hbar g'$ can be intuitively evaluated as

$$\frac{\hbar g'}{\hbar g}=\sqrt{\frac{\sum_{i,j,k}\hat{\Xi}^2_{i,j,k}\left[\mathrm{Im}\left[G_{ij}\right]\right]}{\sum_i\mu_i^2\,\mathrm{Im}\left[G^*_{ii}\right]}} \tag{S17}$$

II. PARITY AND QUANTITY OF MULTIPOLAR MOMENTS

The wave function for electron and hole can be decomposed into the product of Bloch function and envelope function. The Bloch function has odd parity in the direction of dipole transition, while in other directions are even parity. The parity of envelope function are dependent on the shape of QD. For self-assemble InAs/GaAs QD, there is no parity along growth direction due to the structural inhomogeneities, while the parity of two directions inside the growth plane are even [5]. Therefore, given the consideration of the parity selection rules, we find the following non-zero transition moments for x-polarized exciton: μ_x for dipole transition, Λ_{xz} and Λ_{zx} for first-order mesoscopic moment, and $\Omega_{xxx},\Omega_{yyx},\Omega_{zzx},\Omega_{xzz}$ and Ω_{zxz} for the second-order mesoscopic moment. The first- and second-order mesoscopic moment can be rewritten in terms of electric and magnetic contributions. For example, Λ_{xz} contains the electric-quadrupole (EQ) $\mathrm{Q}_{xz}=(e/2m)\left\langle v\left|xp_z+zp_x\right|c\right\rangle$ and the magnetic-dipole $\mathrm{m}_y=(e/2m)\left\langle v\left|xp_z-zp_x\right|c\right\rangle$ contributions. Accordingly, Q_{xz} couples to electric field gradient $\mathrm{Im}\left[\partial_xG_{zx}+\partial_zG_{xx}\right]$, while m_y depends on $\mathrm{Im}\left[\partial_xG_{zx}-\partial_zG_{xx}\right]$. Similarly, one can conclude that the magnetic-quadrupole (MQ) $\widetilde{\mathbf{Q}}_{yy}$ of Ω_{xzz} couples to $\mathrm{Im}\left[2\partial_x\partial_zG_{zx}-\partial_z\partial_xG_{zx}-\partial_z\partial_zG_{xx}\right]$, $\widetilde{\mathbf{Q}}_{yz}$ of Ω_{yyx} depends on $\mathrm{Im}\left[2\partial_y\partial_yG_{xx}-\partial_x\partial_yG_{yx}-\partial_y\partial_xG_{yx}\right]$ and $\widetilde{\mathbf{Q}}_{zy}$ of Ω_{zzx} couples to $\mathrm{Im}\left[2\partial_z\partial_zG_{xx}-\partial_x\partial_zG_{zx}-\partial_z\partial_xG_{zx}\right]$. There is no MQ for Ω_{xxx}. In next section we will show that for plasmonic nanoparticles, only EQ survives in Ω_{yyx}, and the contribution of MQ in Ω_{xzz} and Ω_{zzx} is much smaller than EQ and can be omitted. Therefore, in the main text we call $\Lambda_{ji}(\phi)$ and $\Omega_{kji}(\phi)$ as the equivalent (electric) quadrupole and octupole transition moments, respectively.

To determine the quantity of multipolar transition moments, one only needs to calculate the ratio Λ_{ji}/μ_x and Ω_{kji}/μ_x for the reason that on the one hand, in general μ_x is known; on the other hand, the contribution of multipolar transition can be estimated by $\mu_x\left[1+\left(\Lambda_{ji}/\mu_x\right)\partial_j+\left(\Omega_{kji}/\mu_x\right)\partial_j\partial_k\right]$, once the partial derivative of Green's tensor are known.

Λ_{zx} scales with the height of QD because of $\Lambda_{zx}=(e/m)\left\langle v\left|(z-z_0)\,p_x\right|c\right\rangle$, which is much smaller than Λ_{xz} as it scales with the radius of QD. The evaluation gives $|\Lambda_{zx}/\mu_x|\approx0.1$nm, while $|\Lambda_{xz}/\mu_x|$ is around 10nm of a 15nm-radius QD according to the experimental measurement [5]. But in general it depends on the size, shape and the materials of QD, and hence we evaluate the multipolar moments via modeling the QD as a harmonic in-plane confinement and

an infinite barrier in the z direction [6–8]. The convergence of this multipole expansion approach compared with the fully wavefunction-based computation is shown in Sec. IV.

With the commutation $\left[\widehat{L}_x, r_i\right] = \varepsilon_{xij} i\hbar r_j$ and $\left[\widehat{L}_x, p_i\right] = \varepsilon_{xij} i\hbar p_j$, where ε_{xij} is the Levi-Civita symbol, as well as the identity $e^{\xi\hat{A}}\widehat{B}e^{-\xi\hat{A}} = \widehat{B} + \xi[\hat{A}, \hat{B}] + \frac{\xi^2}{2!}[\hat{A}, [\hat{A}, \widehat{B}]] + \cdots$, where ξ is a c-number, we obtain

$$\mu_x(\phi) = \mu_x \tag{S18}$$

$$\Lambda_{xz}(\phi) = \cos(\phi)\Lambda_{xz} \tag{S19}$$

$$\begin{bmatrix} \Omega_{xxx}(\phi) \\ \Omega_{yyx}(\phi) \\ \Omega_{zzx}(\phi) \\ \Omega_{xzz}(\phi) \end{bmatrix} = \begin{bmatrix} 1 & 0 & 0 & 0 \\ 0 & \cos^2(\phi) & \sin^2(\phi) & 0 \\ 0 & \sin^2(\phi) & \cos^2(\phi) & 0 \\ 0 & 0 & 0 & \cos^2(\phi) \end{bmatrix} \begin{bmatrix} \Omega_{xxx} \\ \Omega_{yyx} \\ \Omega_{zzx} \\ \Omega_{xzz} \end{bmatrix} \tag{S20}$$

Note that $\Omega_{zxz}(\phi)$ is the same as $\Omega_{xzz}(\phi)$. For the electric field expanded as Eq. (S8), the LCS can be collected in the form as

$$\Gamma\left(\mathbf{r}_0, \phi\right) = \Gamma^{(d)}\left(\mathbf{r}_0\right) + \Gamma^{(Q)}\left(\mathbf{r}_0, \phi\right) + \Gamma^{(O)}\left(\mathbf{r}_0, \phi\right) + \Gamma^{(dQ)}\left(\mathbf{r}_0, \phi\right) + \Gamma^{(dO)}\left(\mathbf{r}_0, \phi\right) + \Gamma^{(QO)}\left(\mathbf{r}_0, \phi\right) \tag{S21}$$

For $\Gamma^{(QO)}\left(\mathbf{r}_0, \phi\right)$ and $\Gamma^{(O)}\left(\mathbf{r}_0, \phi\right)$ are respected to the third and fouth derivative of the Green's function and trends to zero, the final form of LCS is

$$\Gamma\left(\mathbf{r}_0, \phi\right) = \Gamma^{(d)}\left(\mathbf{r}_0\right) + \Gamma^{(Q)}\left(\mathbf{r}_0, \phi\right) + \Gamma^{(dQ)}\left(\mathbf{r}_0, \phi\right) + \Gamma^{(dO)}\left(\mathbf{r}_0, \phi\right) \tag{S22}$$

with

$$\Gamma^{(d)}\left(\mathbf{r}_0\right) = A|\mu|^2 \mathrm{ImG}_{\mathrm{xx}}\left(\mathbf{r}_0, \mathbf{r}_0, \omega\right) \tag{S23}$$

$$\Gamma^{(Q)}\left(\mathbf{r}_0, \phi\right) = -A\cos^2(\phi)\left|\Lambda_{xz}\right|^2 \partial_x \partial_x \mathrm{ImG}_{\mathrm{zz}}\left(\mathbf{r}_0, \mathbf{r}_0, \omega\right) \tag{S24}$$

$$\Gamma^{(dQ)}\left(\mathbf{r}_0, \phi\right) = 2A\mathrm{Re}\left[\cos(\phi)\Lambda_{\mathrm{xz}}\mu_{\mathrm{x}}^*\right] \partial_{\mathrm{x}} \mathrm{ImG}_{\mathrm{zx}}\left(\mathbf{r}_0, \mathbf{r}_0, \omega\right) \tag{S25}$$

$$\begin{aligned} \Gamma^{(dO)}\left(\mathbf{r}_0, \phi\right) = & A\left\{2\mathrm{Re}\left[\cos^2(\phi)\Omega_{\mathrm{xzz}}\mu_{\mathrm{x}}^*\right] \partial_{\mathrm{x}}\partial_{\mathrm{z}} \mathrm{ImG}_{\mathrm{zx}}\left(\mathbf{r}_0, \mathbf{r}_0, \omega\right) + \mathrm{Re}\left[\Omega_{\mathrm{xxx}}\mu_{\mathrm{x}}^*\right] \partial_{\mathrm{x}}\partial_{\mathrm{x}} \mathrm{ImG}_{\mathrm{xx}}\left(\mathbf{r}_0, \mathbf{r}_0, \omega\right)\right\} \\ & + A\{\mathrm{Re}\left[\left(\cos^2(\phi)\Omega_{\mathrm{yyx}} + \sin^2(\phi)\Omega_{\mathrm{zzx}}\right)\mu_{\mathrm{x}}^*\right] \partial_{\mathrm{y}}\partial_{\mathrm{y}} + \mathrm{Re}\left[\left(\cos^2(\phi)\Omega_{\mathrm{zzx}} + \sin^2(\phi)\Omega_{\mathrm{yyx}}\right)\mu_{\mathrm{x}}^*\right] \partial_{\mathrm{z}}\partial_{\mathrm{z}}\} \mathrm{ImG}_{\mathrm{xx}}\left(\mathbf{r}_0, \mathbf{r}_0, \omega\right) \end{aligned} \tag{S26}$$

where $A = 2\omega^2/\hbar\varepsilon_0 c^2$, and we discard all terms whose Green's function exceeds the second order.

III. DYADIC GREEN'S FUNCTION OF THREE-LAYERED SPHERICAL SHELL AND NUMERICAL CALCULATION OF LDOS

The electromagnetic Green's function of three-layered spherical shell structure can be analytically obtained. Given a nanoshell with permittivity ε_c of core and ε_m of shell and a source point at $\boldsymbol{r}'$, embedded in a homogeneous medium of permittivity ε_b, the scattered part of the Green's function at $\boldsymbol{r}$ outside the structure is given by [9]

$$\begin{aligned} \mathbf{G}^{\mathrm{S}}\left(\boldsymbol{r}, \boldsymbol{r}', \omega\right) = & \frac{ik_1}{4\pi} \sum_{e,0} \sum_{n=1}^{\infty} \sum_{m=0}^{n} \left(2 - \delta_{0m}\right) \frac{2n+1}{n(n+1)} \frac{(n-m)!}{(n+m)!} \left\{\mathcal{B}_M(\omega) \boldsymbol{M}_{mn}^{e/o}\left(\boldsymbol{r}, k_1\right) \boldsymbol{M}_{mn}^{e/o}\left(\boldsymbol{r}', k_1\right)\right. \\ & \left. + \mathcal{B}_N(\omega) \boldsymbol{N}_{mn}^{e/o}\left(\boldsymbol{r}, k_1\right) \boldsymbol{N}_{mn}^{e/o}\left(\boldsymbol{r}', k_1\right)\right\} \end{aligned} \tag{S27}$$

where $k_1 = \frac{\omega}{c}\sqrt{\varepsilon_b}$, m and n identify the eigenvalue parameters. $\mathcal{B}_M/\mathcal{B}_N$ are the coefficients corresponding to transverse electric/magnetic (TE/TM) waves, and $\boldsymbol{M}_{mn}^{e/o}/\boldsymbol{N}_{mn}^{e/o}$ are the spherical vector wave functions corresponding to TE/TM waves and separated into even and odd modes. The values of $\mathcal{B}_M/\mathcal{B}_N$ are given by

$$\mathcal{B}_M(\omega) = -\frac{k_2 I_{11}\left[\partial\Im_{21} - \partial\hbar_{21}\mathcal{R}_M(\omega)\right] - k_1\partial\Im_{11}\left[\widetilde{\gamma}_{21} - \hbar_{21}\mathcal{R}_M(\omega)\right]}{k_2\hbar_{11}\left[\partial\Im_{21} - \partial\hbar_{21}\mathcal{R}_M(\omega)\right] - k_1\partial\hbar_{11}\left[\widetilde{\gamma}_{21} - \hbar_{21}\mathcal{R}_M(\omega)\right]} \tag{S28}$$

$$\mathcal{B}_N(\omega) = -\frac{k_2\partial\Im_{11}\left[\Im s_{21} - \hbar_{21}\mathcal{R}_N(\omega)\right] - k_1\Im\Im_{11}\left[\partial\Im\Im_{21} - \partial\hbar_{21}\mathcal{R}_N(\omega)\right]}{k_2\partial\hbar_{11}\left[\widetilde{\Im}_{21} - \hbar_{21}\mathcal{R}_N(\omega)\right] - k_1\hbar_{11}\left[\partial\Im_{21} - \partial\hbar_{21}\mathcal{R}_N(\omega)\right]} \tag{S29}$$

where $k_2 = \frac{\omega}{c}\sqrt{\varepsilon_m}$, $k_3 = \frac{\omega}{c}\sqrt{\varepsilon_c}$ and the coefficients

$$\mathcal{R}_M(\omega) = \frac{k_3\widetilde{\Im}_{22}\partial\Im_{32} - k_2\widetilde{\Im}_{32}\partial\Im_{22}}{k_3\hbar_{22}\partial\Im_{32} - k_2\widetilde{\Im}_{32}\partial\hbar_{22}} \tag{S30}$$

$$\mathcal{R}_N(\omega) = \frac{k_3\Im_{32}\partial\Im_{22} - k_2\widetilde{\Im}_{22}\partial\Im_{32}}{k_3\Im s_{32}\partial\hbar_{22} - k_2\hbar_{22}\partial\Im_{32}} \tag{S31}$$

with

$$\Im_{il} = j_n\left(k_i r_l\right), \quad \hbar_{il} = h_n^{(1)}\left(k_i r_l\right) \tag{S32}$$

$$\partial\Im_{il} = \frac{1}{\rho}\frac{d\left[\rho j_n(\rho)\right]}{d\rho}\bigg|_{\rho=k_i r_l}, \quad \partial\hbar_{il} = \frac{1}{\rho}\frac{d\left[\rho h_n^{(1)}(\rho)\right]}{d\rho}\bigg|_{\rho=k_i r_l} \tag{S33}$$

where j_n and $h_n^{(1)}$ are the spherical Bessel functions and the spherical Hankel function of the first kind, respectively. The vector functions are defined as

$$\boldsymbol{M}_{mn}^{e}(\boldsymbol{r},k) = -\frac{m}{\sin\theta}h_n^{(1)}(kr)P_n^m(\cos\theta)\sin m\varphi\widehat{\boldsymbol{\theta}} - h_n^{(1)}(kr)\frac{dP_n^m(\cos\theta)}{d\theta}\cos m\varphi\widehat{\boldsymbol{\varphi}} \tag{S34}$$

$$\boldsymbol{M}_{mn}^{o}(\boldsymbol{r},k) = \frac{m}{\sin\theta}h_n^{(1)}(kr)P_n^m(\cos\theta)\cos m\varphi\widehat{\boldsymbol{\theta}} - h_n^{(1)}(kr)\frac{dP_n^m(\cos\theta)}{d\theta}\sin m\varphi\widehat{\boldsymbol{\varphi}} \tag{S35}$$

$$\begin{aligned}\boldsymbol{N}_{mn}^{e}(\boldsymbol{r},k) = {} & \tfrac{n(n+1)}{kr}h_n^{(1)}(kr)P_n^m(\cos\theta)\cos m\varphi\hat{\boldsymbol{r}} + \tfrac{1}{kr}\tfrac{d\left[rh_n^{(1)}(kr)\right]}{dr}\tfrac{dP_n^m(\cos\theta)}{d\theta}\cos m\varphi\widehat{\boldsymbol{\theta}} \\ & - \tfrac{m}{kr\sin\theta}\tfrac{d\left[rh_n^{(1)}(kr)\right]}{dr}P_n^m(\cos\theta)\sin m\varphi\widehat{\boldsymbol{\varphi}}\end{aligned} \tag{S36}$$

$$\begin{aligned}\boldsymbol{N}_{mn}^{o}(\boldsymbol{r},k) = {} & \tfrac{n(n+1)}{kr}h_n^{(1)}(kr)P_n^m(\cos\theta)\sin m\varphi\hat{\boldsymbol{r}} + \tfrac{1}{kr}\tfrac{d\left[rh_n^{(1)}(kr)\right]}{dr}\tfrac{dP_n^m(\cos\theta)}{d\theta}\sin m\varphi\widehat{\boldsymbol{\theta}} \\ & + \tfrac{m}{kr\sin\theta}\tfrac{d\left[rh_n^{(1)}(kr)\right]}{dr}P_n^m(\cos\theta)\cos m\varphi\widehat{\boldsymbol{\varphi}}\end{aligned} \tag{S37}$$

where P_n^m are the associated Legendre polynomials.

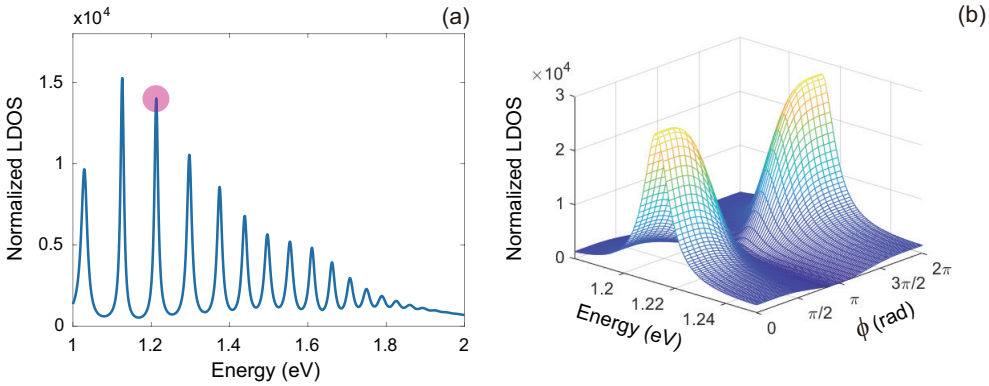

FIG. S2. (a) Normalized LDOS of QD with a dipole transition moment parallel to the metallic surface at $s = 2$nm under the dipole approximation. (b) Normalized LDOS of the plasmonic mode indicated by the pink circle in (a) with nondipole effect and QD radius $R = 6$nm.

The local density of photonic states (LDOS) for a QD 2nm away from the nanoshell with a dipole transition moment parallel to the metallic surface is shown in Fig. S2(a). Metallic nanoshell structures have two sets of modes, separated

by surface plasmon frequency ω_{SP}: the modes whose peaks locates above ω_{SP} are called cavity-like modes, while those modes with peak frequency below ω_{SP} are sphere-like modes [10, 11]. We have tuned the lowest sphere-like mode to match the emission energy of QD, which is $\hbar\omega_0 = 1.213$eV, with the parameters given in the main text. The normalized LDOS of the third sphere-like mode for $s = 2$nm with nondipole effect of a 6nm-radius QD is shown in Fig. S2(b). For calculating the partial derivative of Green's function, the spatial interval $\Delta x = \Delta y = \Delta z = 5 \times 10^{-3}$nm is used.

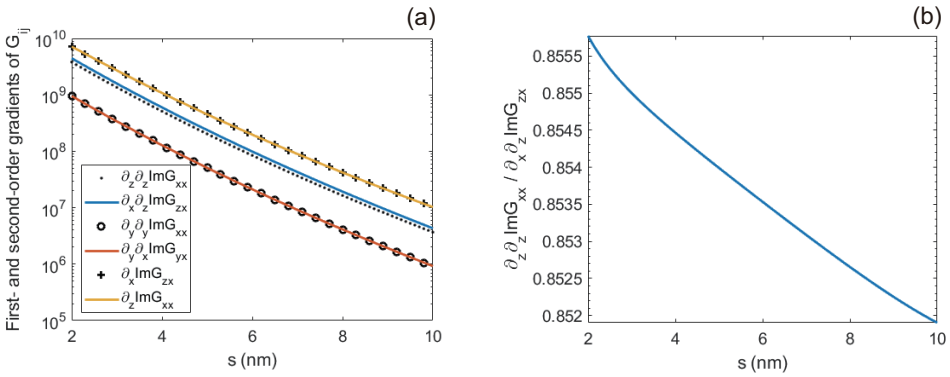

FIG. S3. First- and second-order gradients of G_{ij} (a) and $\partial_z\partial_z G_{xx}/\partial_x\partial_z G_{zx}$ (b) as the function of QD-nanoshell separation s at the QD emission wavelength. Nanoshell parameters are the same as Fig. S2.

Fig. S3(a) compares $\partial_y\partial_y G_{xx}$ with $\partial_x\partial_y G_{yx}$, $\partial_z\partial_z G_{xx}$ with $\partial_x\partial_z G_{zx}$ as well as $\partial_x G_{zx}$ with $\partial_z G_{xx}$. We can see that for nanoshell $\partial_y\partial_y G_{xx}$ and $\partial_z G_{xx}$ are exactly equal to $\partial_x\partial_y G_{yx}$ and $\partial_x G_{zx}$, respectively, leading to the completely electric-transition contributions in Λ_{xz} and Ω_{yyx}. While $\partial_x\partial_z G_{zx}$ is slightly larger than $\partial_z\partial_z G_{xx}$, and their ratio $\alpha = \partial_z\partial_z G_{xx}/\partial_x\partial_z G_{zx}$ is shown in Fig. S3(b), where we can see $\alpha \approx 0.854$ for $2nm < s < 10nm$. Then we can evaluate the ratio of electric contribution to magnetic contribution in Ω_{zzx} and Ω_{xzz} as $(1+\alpha)/(1-\alpha) \approx 12$. Therefore, the MQ contributions of Ω_{zzx} and Ω_{xzz} can be omitted.

The LDOS of the model in Fig. 3(d) in the main text is numerically calculated by MNPBEM toolbox, which is based on boundary element method (BEM) [12]. The radius and height of GaAs cylinder are R and $4R$. A dipole source is placed at the center of the cylinder to evaluate the LDOS. The nanoshell is embedded in the GaAs substrate with a separation of R from the dipole.

IV. CONVERGENCE OF MULTIPOLE EXPANSION

For the QDs with lattice distortion, the LCS is expressed as [13]

$$\begin{aligned}\Gamma^I(\omega) = C\int d^3\mathbf{r}\int d^3\mathbf{r}'\mathrm{Im}\left[J_x(\mathbf{r})\mathrm{G_{xx}}\left(\mathbf{r},\mathbf{r}',\omega\right)J_x{}^*\left(\mathbf{r}'\right)\right] + 2C\mathrm{Re}\left[\int \mathrm{d}^3\mathbf{r}\int \mathrm{d}^3\mathbf{r}'\mathrm{Im}\left[J_x(\mathbf{r})\mathrm{G_{xz}}\left(\mathbf{r},\mathbf{r}',\omega\right)J_z^*\left(\mathbf{r}'\right)\right]\right] \\ + C\int d^3\mathbf{r}\int d^3\mathbf{r}'\,\mathrm{Im}\left[J_z(\mathbf{r})\mathrm{G_{zz}}\left(\mathbf{r},\mathbf{r}',\omega\right)J_z^*\left(\mathbf{r}'\right)\right]\end{aligned} \tag{S38}$$

where $C = 2\mu_0 e\left|\boldsymbol{p}_{cv}\right|^2/m_0\hbar$, μ_0 is the permeability of vacuum and Bloch matrix element $\boldsymbol{p}_{cv} = \frac{1}{v_{UC}}\int_{\mathrm{UC}} d^3\mathbf{r}u_e(\mathbf{r})\mathbf{p}u_h(\mathbf{r})$ is a material parameter. $J_x(\mathbf{r}) = \chi(\mathbf{r})$ and $J_z(\mathbf{r}) = xk_l^{-1}\left(\partial k_l/\partial z\right)\chi(\mathbf{r})$, where $k_l = 2\pi/a$ is the lattice wave vector and $\chi(\mathbf{r})$ is the exciton envelope function. In the calculation we assump that: (i) the dipole orientation is along x direction, (ii) the exciton with a Gaussian envelope function and (iii) $\partial k_l/\partial z = \Delta a\delta\left(z - z_0\right)$, where delta function is approached by $\delta\left(z - z_0\right) = \left(\Delta z\sqrt{\pi}\right)^{-1}e^{-(z-z_0)^2/\Delta z^2}$. We use the parameters $a/\Delta a = 0.18$ and $z_0 = 0$ [13].

The normalized LDOS for self-assemble InAs/GaAs QD is

$$\rho^{\mathrm{InAs}} = \frac{\Gamma^I(\omega)}{C\left|\int d^3\mathbf{r}\chi(\mathbf{r})\right|^2\mathrm{Im}\left[\mathbf{n_x}\cdot\mathbf{G}\left(\mathbf{r}_0,\mathbf{r}_0,\omega\right)\cdot\mathbf{n_x}\right]} \tag{S39}$$

Eq. (S38) is the exact expression of the normalized DOS including nondipole effects. In Fig. S4 we compare the results of Eq. (S39) with that using multipole expansion, i.e., replace $\Gamma^I(\omega)$ in Eq. (S39) by Eq. (S22).

For a QD without lattice distortion, the normalized LDOS with nondipole effects is

$$\rho^{\mathrm{CdSe}} = \frac{\int d^3\mathbf{r}\int d^3\mathbf{r}'\chi(\mathbf{r})\chi\left(\mathbf{r}'\right)\mathrm{Im}\left[\mathbf{n}_i\cdot\mathbf{G}\left(\mathbf{r},\mathbf{r}',\omega\right)\cdot\mathbf{n}_i\right]}{\left|\int d^3\mathbf{r}\chi(\mathbf{r})\right|^2\mathrm{Im}\left[\mathbf{n}_i\cdot\mathbf{G}\left(\mathbf{r}_0,\mathbf{r}_0,\omega\right)\cdot\mathbf{n}_i\right]} \tag{S40}$$

where i represents the dipole orientation. The convergence of multipole expansion for a 5nm-radius spherical CdSe QD with different deformations are shown in Fig. S5. Fig. S5(f) shows the exact results of $\Gamma^{\mathrm{N}} = \Gamma/\Gamma^{(d)}$ for an idealized spherical QD. The deviation from point-dipole is too small to observe in normalized LDOS in Fig. S5(c).

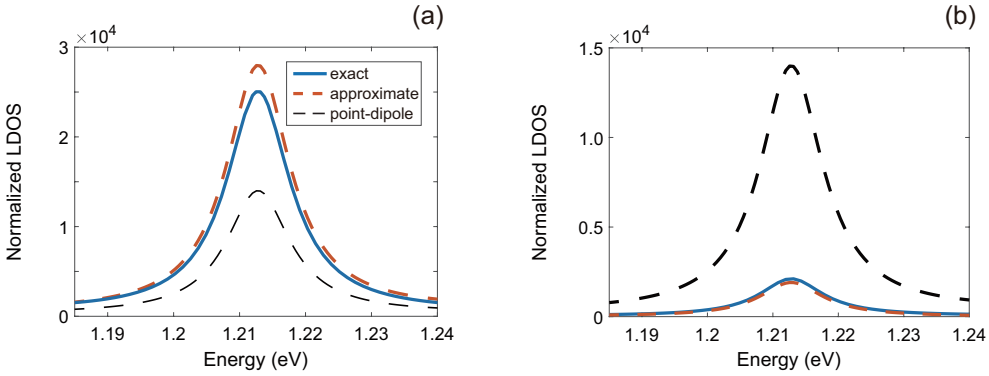

FIG. S4. Normalized LDOS beyond the point-dipole approximation for self-assemble InAs/GaAs QD as the function of wavelength for $\phi = 0$ (a) and $\phi = \pi$ (b). Other parameters are $s = 2$nm and $R = 6$nm.

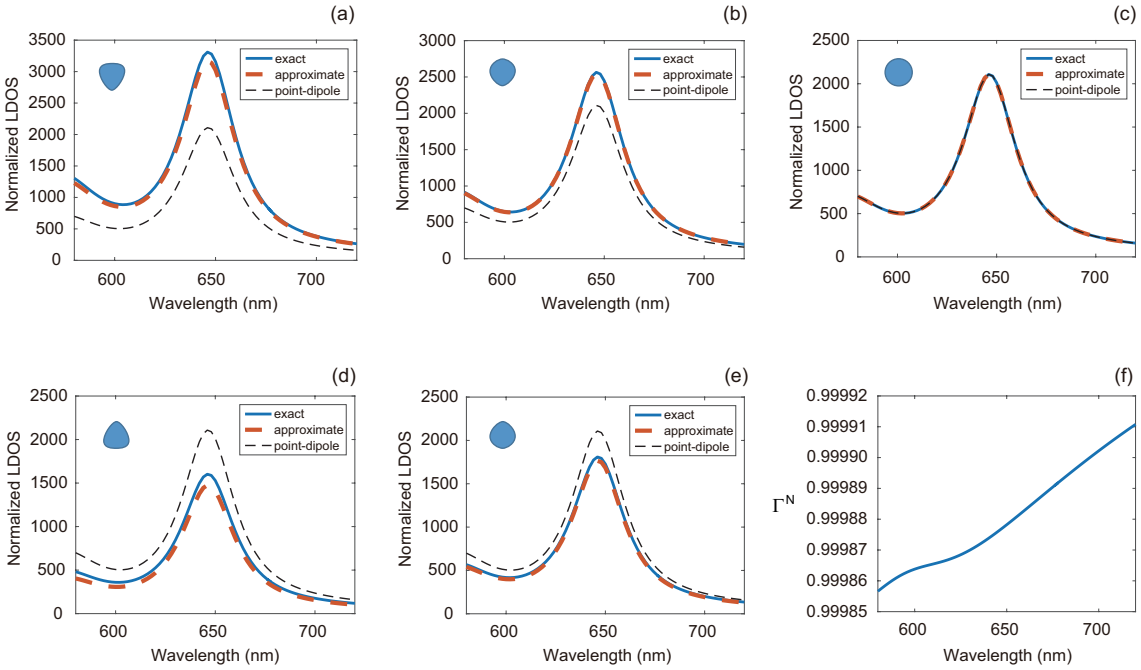

FIG. S5. Normalized LDOS beyond the point-dipole approximation for CdSe QDs as the function of wavelength for $s = 7$nm and $R = 5$nm. (a)-(e) are for QDs with different deformations. The geometric shape of QDs are illustrated by the blue objects at the top left corner in figures. Particularly, (c) is an idealized spherical QD. (d) and (e) are actually fliping the QD in (a) and (b) top to bottom, respectively. (f) is the enhancement of decay rate $\Gamma^N = \Gamma/\Gamma^{(d)}$ versus wavelength for an idealized spherical CdSe QD.

V. TRAJECTORIES OF ENCIRCLING THE EXCEPTIONAL POINT

In this section we show how to use the nondipole effect of mesoscopic QD to encircle the exceptional point (EP) to reveal this topological property.

By phenomenologically introducing the effective decay rate κ of cavity and spontaneous emission rate γ of QD, the coupled system can be treated by a non-Hermitian Hamiltonian in the Jaynes-Cummings form, which in the single-excitation subspace can be described by the matrix [14]

$$H_n = \begin{pmatrix} \omega_0 - i\frac{\gamma}{2} & g \\ g & \omega_c - i\frac{\kappa}{2} \end{pmatrix} \tag{S41}$$

where ω_c and g are the resonant frequency of silver nanoshell and the coupling coefficient of plasmon-QD interaction, respectively. The diagonalization of H_n yields the eigenenergies

$$\omega_\pm = \frac{1}{2}(\omega_0 + \omega_c) - i\frac{\gamma+\kappa}{4} \pm \sqrt{g^2 + \left(i\frac{\gamma-\kappa}{4} + \frac{\omega_0-\omega_c}{2}\right)^2} \tag{S42}$$

In resonant coupling ($\omega_0 = \omega_c$), the critical point between the strong- and the weak-coupling regime is the EP, the corresponding coupling strength is $g_{EP} = (\kappa-\gamma)/4$. Expressing the perturbation of coupling strength as $\epsilon = g - g_{EP}$, the eigenenergies spacing $\Delta = \mathrm{Re}[\omega_+ - \omega_-]$ around the EP can be found as $\Delta = 2\sqrt{(2g_{EP}+\epsilon)\,\epsilon}$. Around the EP $\epsilon \ll g_{EP}$, we have $\Delta_{EP} = \sqrt{2(\kappa-\gamma)}\sqrt{\epsilon}$. While far from the EP,$\epsilon \gg 2g_{EP}$ gives $\Delta_{\text{Linearity}} = 2\epsilon$.

Based on the pseudomodes method [15, 16], the cavity parameters ω_c, g and κ can be obtained by fitting the LCS $\Gamma(\mathbf{r}_0,\omega)$ with Lorentz function $g^2\frac{\kappa}{(\omega-\omega_c)^2+(\kappa/2)^2}$. On the other hand, the singular point of SE spectrum $C_e(\omega)$, which is the root of the denominator in Eq. (S14), yields $\omega - \omega_0 + i\gamma/2 = \Delta(\mathbf{r}_0,\omega) - i\Gamma(\mathbf{r}_0,\omega)/2$. With the same Lorentzian fitting parameters, we have

$$\Delta(\mathbf{r}_0,\omega) - \frac{i\Gamma(\mathbf{r}_0,\omega)}{2} = g^2\frac{\omega-\omega_c-i\kappa/2}{(\omega-\omega_c)^2+(\kappa/2)^2} \tag{S43}$$

and thus

$$\omega_\pm = \frac{1}{2}(\omega_0 + \omega_c) - i\frac{\gamma+\kappa}{4} \pm \sqrt{g'^2 + \left(i\frac{\gamma+\kappa}{4} + \frac{\omega_0-\omega_c}{2}\right)^2} \tag{S44}$$

We can see the eigenenergies are identical with the non-Hermitian Hamiltonian. The Rabi splitting in SE spectrum reflects the eigenenergies of H_n.

For the LDOS shown in Fig. S2, we obtain the coupling coefficient $\hbar g = 5.1$meV and plasmonic cavity relaxation $\hbar\kappa = 12.56$meV in dipole approximation when $s = 3.5$nm. The coupling coefficient $\hbar g'$ beyond the dipole approximation can be obtained from Eq. (S17), and shown in Fig. S6.

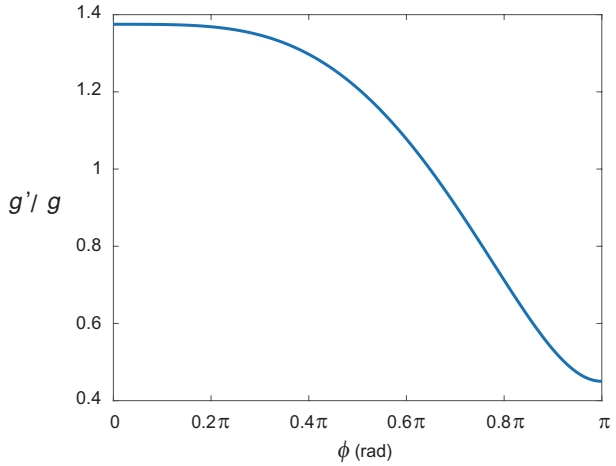

FIG. S6. g'/g as a funtion of ϕ for $s = 4$nm and $R = 6$nm.

For two coupled subsystems, an EP is at the critical coupling between the strong and weak coupling at zero detuning. Therefore, we need to tune the coupling strength and switch between the strong and weak coupling to encircle an EP. For $s = 3.5$nm the critical coupling strength is about 3.1meV, corresponding to $\phi = 0.85\pi$; the paramter ϕ we choose for strong coupling and weak coupling under a cyclic variation in parameter space $(\Delta\omega, \phi)$ are $\phi = 0.72\pi$

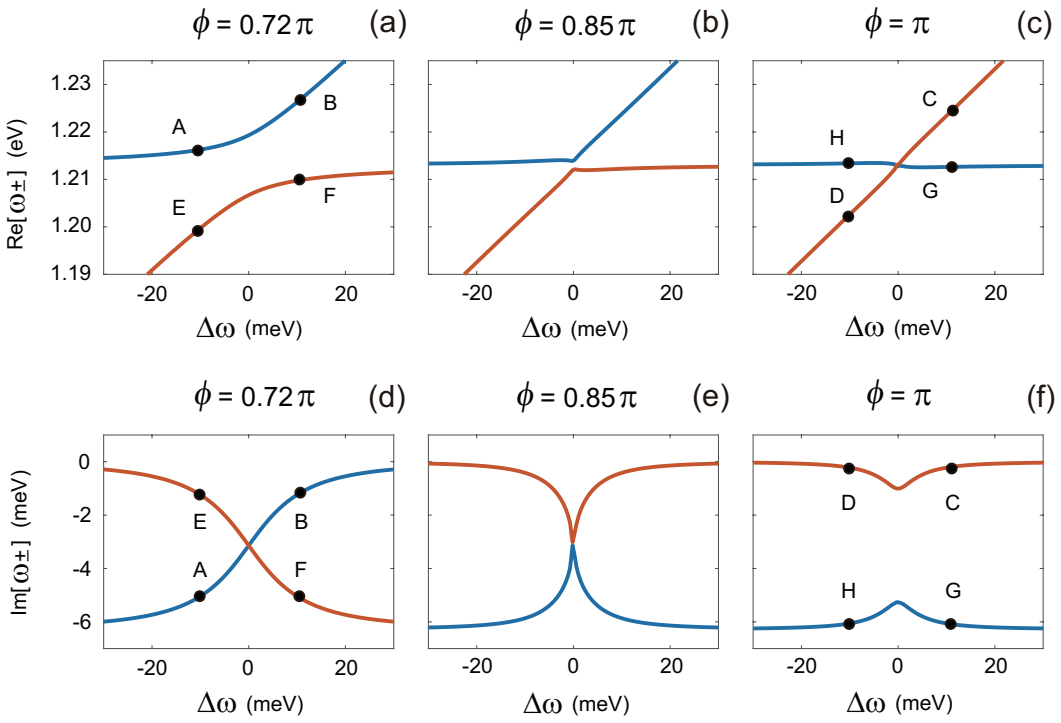

FIG. S7. (a)-(c) Real part of the eigenenergies as the function of detunings for $\phi = 0.72\pi$ (strong coupling), 0.85π (EP condition) and π (weak coupling) when $s = 3.5$nm and $R = 6$nm, respectively. (d)-(f) show the imaginary part of the eigenenergies. The blue and orange lines show the two eigenstates of polariton.

($\hbar g' = 4.5$meV) and $\phi = \pi$ ($\hbar g' = 2.3$meV), respectively. The eigenenergies for these three ϕ when $\Delta\omega$ is varied are shown in Fig. S6. Suppose we start encircling the EP from $\mathbf{A}(-10, 0.72\pi)$ at an eigenstate colored blue in Fig. S7, after a 2π rotation: $\mathbf{B}(10, 0.72\pi) \to \mathbf{C}(10, \pi) \to \mathbf{D}(-10, \pi) \to \mathbf{E}(-10, 0.72\pi)$, we end up with another eigenstate (the orange one); continuelly rotate another 2π: $\mathbf{F}(10, 0.72\pi) \to \mathbf{G}(10, \pi) \to \mathbf{H}(-10, \pi) \to \mathbf{A}(-10, 0.72\pi)$, now we arrive at the initial point.

VI. FORMATION OF THREE-ORDER EPS BY TWO QDS

This section derives the critical coupling strengths for forming the three-order EPs (EP3) by resonantly coupling two QDs to nanoshell. The non-Hermitian Hamiltonian in the single-excitation subspace is given by

$$H_n^2 = \begin{pmatrix} \omega_c - i\frac{\gamma_1}{2} & g_1 & 0 \\ g_1 & \omega_c - i\frac{\kappa}{2} & g_2 \\ 0 & g_2 & \omega_c - i\frac{\gamma_2}{2} \end{pmatrix} \tag{S45}$$

where $\gamma_{1,2}$ and $g_{1,2}$ are the decaying and the coupling strength with plasmon of two QDs, respectively. Denoting the characteristic polynomial of Eq. (S45) as $P(\omega)$, the eigenenergy of EP3 can be found by letting $\mathrm{P}''(\omega) = 0$. The solution is

$$\omega_{EP} = \omega_c - i\frac{\kappa + \gamma_1 + \gamma_2}{6} \tag{S46}$$

Substituting back into $P(\omega)$, the corresponding coupling strengths can be found as

$$g_{EP}^1 = \frac{\sqrt{\kappa + \gamma_2}}{6}\sqrt{\frac{\kappa + \gamma_2 - 2\gamma_1}{\gamma_1 - \gamma_2}}\sqrt{\kappa + 4\gamma_1 + \gamma_2} \tag{S47}$$

$$g_{EP}^2 = \frac{\sqrt{\kappa + \gamma_1}}{6}\sqrt{\frac{\kappa + \gamma_1 - 2\gamma_2}{\gamma_2 - \gamma_1}}\sqrt{\kappa + \gamma_1 + 4\gamma_2} \tag{S48}$$

We can see that in general it requires $\gamma_1 \neq \gamma_2$ and thus $g_{EP}^1 \neq g_{EP}^2$.

VII. NONDIPOLE EFFECT INDUCED BY NON-SPHERICAL SHAPE

A previous study has rigorously proved that for an idealized spherical QD the LCS is equal to that of a point-dipole [17]. Fig. S8(a) shows a QD with deformation in dipole orientation which is perpendicular to metallic interface shows striking non-dipole effects: more than 60% enhancement or 30% reducing of the LCS can be observed according to different QD orientation (see the blue and green lines). On the other hand, only smaller non-dipole effect can be found for the QD with in-plane (perpendicular to the dipole orientation) deformation, which is less than 4%, as Fig. S8(b) shown. This great distinction is mainly due to whether the deformation breaks the symmetry of QD: for a QD envelope function with even parity the quadrupole moment is vanishing in multipole expansion while the octupole survives. The convergence of multipole expansion have been shown in Sec. IV.

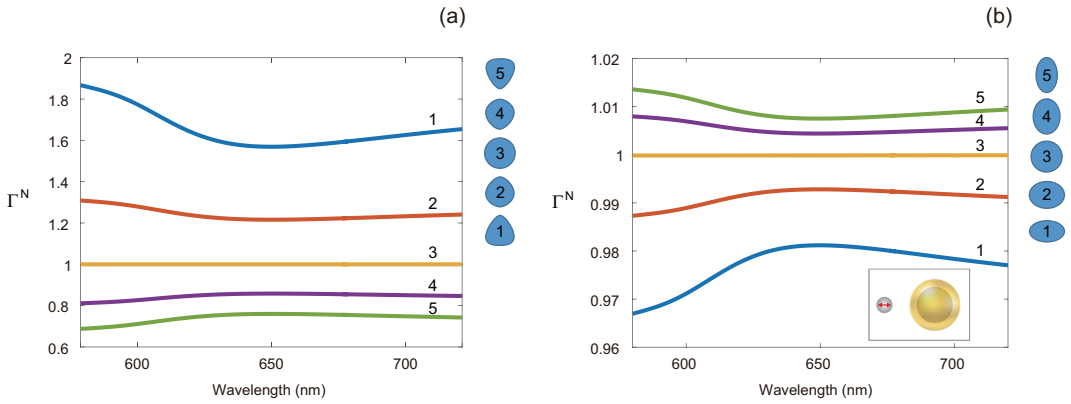

FIG. S8. The enhancement of LCS $\Gamma(\mathbf{r}_0,\phi)/\Gamma^{(d)}(\mathbf{r}_0,\phi)$ versus wavelength of 5nm-radius CdSe QDs located 7nm from the gold nanoshell with deformation along (a) and perpendicular to (b) its dipole orientation. The inset at the bottom right corner in (b) schematically illustrates a CdSe QD coupled to a gold nanoshell. Its dipole orientation points towards the center of nanoshell, and is indicated by the red arrow. The nanoshell with external radius r_1=14nm and internal radius r_2=12nm. The dielectric permittivity of gold is taken from Ref. [18], and the permittivity of the core is $\varepsilon_c = 1.82$. The insets at the right side of figures illustrate the QDs with different deformation, while the number upon the line indexes the corresponding QD.

[1] S. Y. Buhmann, *Dispersion Forces I* (Springer, Berlin, 2012).
[2] P. W. Atkins and R. S. Friedman, *Molecular quantum mechanics*, 4th ed. (Oxford University Press, Oxford, 2005) pp. xiv, 573 p.
[3] X.-H. Wang, B.-Y. Gu, R. Wang, and H.-Q. Xu, Decay kinetic properties of atoms in photonic crystals with absolute gaps, Physical Review Letters **91**, 113904 (2003).
[4] Y.-C. Yu, J.-F. Liu, X.-L. Zhuo, G. Chen, C.-J. Jin, and X.-H. Wang, Vacuum rabi splitting in a coupled system of single quantum dot and photonic crystal cavity: effect of local and propagation green's functions, Optics Express **21**, 23486 (2013).
[5] M. L. Andersen, S. Stobbe, A. S. Sørensen, and P. Lodahl, Strongly modified plasmon–matter interaction with mesoscopic quantum emitters, Nature Physics **7**, 215 (2010).
[6] M. Sugawara, Theory of spontaneous-emission lifetime of wannier excitons in mesoscopic semiconductor quantum disks, Physical Review B **51**, 10743 (1995).
[7] W. Que, Excitons in quantum dots with parabolic confinement, Physical Review B **45**, 11036 (1992).
[8] S. Stobbe, P. T. Kristensen, J. E. Mortensen, J. M. Hvam, J. Mørk, and P. Lodahl, Spontaneous emission from large quantum dots in nanostructures: Exciton-photon interaction beyond the dipole approximation, Physical Review B **86** (2012).
[9] L. Le-Wei, K. Pang-Shyan, L. Mook-Seng, and Y. Tat-Soon, Electromagnetic dyadic green's function in spherically multi-layered media, IEEE Transactions on Microwave Theory and Techniques **42**, 2302 (1994).
[10] F. Alpeggiani, S. D'Agostino, and L. C. Andreani, Surface plasmons and strong light-matter coupling in metallic nanoshells, Physical Review B **86**, 035421 (2012).
[11] J. Hakami and M. S. Zubairy, Nanoshell-mediated robust entanglement between coupled quantum dots, Physical Review A **93**, 022320 (2016).
[12] U. Hohenester and A. Trügler, Mnpbem – a matlab toolbox for the simulation of plasmonic nanoparticles, Computer Physics Communications **183**, 370 (2012).
[13] P. Tighineanu, A. Sørensen, S. Stobbe, and P. Lodahl, Unraveling the mesoscopic character of quantum dots in nanophotonics, Physical Review Letters **114**, 247401 (2015).

[14] H. J. Carmichael, *Statistical Methods in Quantum Optics 1* (Springer, Berlin, Heidelberg, 1999).
[15] S. Hughes, M. Richter, and A. Knorr, Quantized pseudomodes for plasmonic cavity qed, Optics Letters **43**, 1834 (2018).
[16] D. Tamascelli, A. Smirne, S. F. Huelga, and M. B. Plenio, Nonperturbative treatment of non-markovian dynamics of open quantum systems, Physical Review Letters **120**, 030402 (2018).
[17] P. T. Kristensen, J. E. Mortensen, P. Lodahl, and S. Stobbe, Shell theorem for spontaneous emission, Physical Review B **88**, 205308 (2013).
[18] P. B. Johnson and R. W. Christy, Optical constants of the noble metals, Physical Review B **6**, 4370 (1972).